VARIATION OF FRICTION DRAG VIA SPANWISE TRANSVERSAL SURFACE WAVES

S. Klumpp, B. Roidl, W. Schröder, M. Meinke
Institute of Aerodynamics
RWTH Aachen University
Wüllnerstr. 5a, 52062 Aachen, Germany
office@aia.rwth-aachen.de

ABSTRACT

The introduction of spanwise velocity fluctuations is a promising technique to influence the near-wall turbulent flow field such that friction drag is reduced. The essential physical mechanisms which significantly reduce the drag, however, have not been completely understood, yet. It is the objective of this numerical study to improve the fundamental knowledge of the mechanisms involved. The investigation is based on numerical solutions of flows over spanwise traveling transversal surface waves which are applied to modify the near-wall flow field. Two actuation configurations are analyzed in detail and compared with an unactuated flat plate boundary layer simulation. The damping of the wall-normal vorticity fluctuations above the entire surface and the decrease of turbulence production are identified as the two key features for drag reduction.

Introduction

In most high-speed flows over slender bodies such as wings the developing boundary layers are fully turbulent and it is known that shape optimization of the moving bodies can considerably reduce the pressure drag. The viscous drag, however, which is mainly determined by the wetted surface area, cannot be influenced easily. Approximately 50% of the total drag of the flow field around aircraft is determined by the wall-shear stress distribution, i.e., by the friction drag. From this fact and from the immediate link between drag and pollution it is clear that decreased drag results in lower emission, in other words, in a more environmentally friendly or green aircraft [1].

Several numerical and experimental investigations using miscellaneous approaches of inducing wall-normal and/or spanwise velocity components into the near-wall flow field were performed in order to reduce the friction drag in a turbulent near wall flow. Du *et al.* [2] introduced spanwise traveling wave excitations via volume forces to yield a reduction of friction drag by up to 30 %. They found drag reduction with particular combinations of frequency, force magnitude, and energy input of the excitation, whereas other combinations even led to drag increase. By introducing spanwise traveling wave excitation through spanwise motions of a flexible wall with a spanwise wavelength of $\lambda^+ = 1131$ wall units, Zhao *et al.* [3] found the friction drag of a turbulent channel flow to be also reduced by about 30%. Itoh *et al.* [4] determined in an experimental investigation of a flat plate boundary layer at a Reynolds number based on the momentum thickness of $Re_\Theta \approx 1000$ a friction drag reduction by the transversal sinusoidal wall oscillation to be about 7% at a spanwise excitation wavelength of $\lambda^+ \approx 3270$ wall units and a wave amplitude of $y^+ \approx 20$ wall units.
Klumpp *et al.* [5, 6] performed a numerical simulation of a spatially evolving turbulent boundary layer over spanwise traveling transversal sinusoidal surface waves. The setup with an amplitude of $y^+ \approx 30$, a spanwise wavelength of $\lambda^+ \approx 870$, and a period of $T^+ = 50$ led to a friction drag reduction compared to the uncontrolled case of 9%. The determined near-wall secondary flow field, i.e., areas of a non-zero spanwise velocity component, was similar to the distributions caused by the excitation mechanisms of Du *et al.* [2] and Zhao *et al.* [3]. The analysis of the near-wall structure of the controlled flow showed similar distributions of the secondary flow field and ribbon-like structures of the streamwise vorticity and damped wall-normal vorticity fluctuations as in [2]. It has to be emphasized, however, that it remains still unclear which of these effects causes the reduction of friction drag.

In this paper the results of turbulent flat plate boundary-layer flows actuated via two different spanwise transversal surface wave configurations are analyzed and compared with a corresponding unactuated boundary-layer flow to gain more insight into the mechanisms which lead to drag reduction.

Numerical Method and Computational Setup

The Navier-Stokes equations are solved for three-dimensional compressible flow with a monotone-integrated large-eddy simulation (MILES) [7]. The discretization of the inviscid terms consists of a mixed centered-upwind AUSM (advective upstream splitting method) scheme [8] at second-order accuracy and the viscous terms are discretized second-order accurate using a centered approximation. The temporal integration is done by a second-order explicit 5-stage Runge-Kutta method. For a detailed description of the method the reader is referred to Meinke *et al.* [9] and a thorough discussion of the quality of its solutions in fully turbulent low Mach number flows is discussed, for instance, in [10, 11].

The inflow conditions of a fully turbulent boundary layer are prescribed via an auxiliary flat plate flow simulation which generates its own turbulent inflow data using the compressible rescaling method proposed by El-Askary *et al.* [12]. In the spanwise direction, fully periodic boundary conditions are used. The outflow boundary conditions are based on the conservation equations written in characteristic variables. A sponge layer is used to damp numerical reflections on the upper and outflow boundaries. On the wall, the no-slip conditions are prescribed. The velocity matches the wall velocity, which becomes non-zero in case of a moving wall. The computational setup is visualized in Figure 1. At all performed simulations the Reynolds number is set to $Re_{\delta,i} = U_\infty \delta_i/\nu = 1000$, where U_∞ denotes the freestream velocity and δ_i the displacement thickness of the boundary layer at the inlet of the computational domain used for the boundary rescaling simulation (RS).

A summary of all grid parameters is given in Table 1. Note that the near-wall resolution is similar to that of a direct numerical simulation (DNS). A very fine resolution has been chosen in this area to ensure a proper simulation of the impact of the wall actuation on the turbulent structures. However, the overall resolution does not satisfy the DNS requirements which is why the LES notation is used for the discussion of the results in this paper.

The actual wall position for an actuated wall is prescribed as a function of the spanwise position z and the time t by

$$y(z,t) = \hat{y}\sin\left(\frac{2\pi}{\lambda_z}z - \frac{2\pi}{T}t\right), \tag{1}$$

where the spanwise wavelength of the surface wave is denoted by z, the period by T, and the wave amplitude by y. A sketch of the actuated wall of the domain is given in Figure 2.

Two setups of wall oscillation are investigated, which are denoted as actuated wall case 1 (AWC1) and actuated wall case 2 (AWC2). The AWC1 case matches the setup used in [5]. The AWC2 configuration ($\hat{y}^+$=30, λ^+=174, T^+=10) possesses a smaller amplitude, wavelength, and period compared to the AWC1 case ($\hat{y}^+$=30, λ^+=870, T^+=50).

Results

The solution for case AWC1 possesses a time averaged friction drag more than 9% smaller than the unactuated wall, whereas the time averaged friction drag of the AWC2 setup is increased by about 8% compared to the unactuated wall. These are not the maximum values which can be achieved by the wall actuation, but these two cases contain the main mechanisms which define higher or lower drag.

The secondary flow fields introduced by spanwise traveling transversal surface waves are illustrated in Figure 3 and Figure 4 for case AWC1 and AWC2, respectively. A qualitatively similar secondary flow field is evident for both wavy setups AWC1 and AWC2. At both oscillation configurations the layer above the wall which possesses a non-zero net spanwise fluid transport grows in the streamwise direction. Although, the wall moves only in the y-direction, the spanwise traveling wave produces a net spanwise fluid transport in the positive spanwise direction which corresponds to the propagation direction of the surface wave. At AWC1 the maximum spanwise velocity is approximately 3% of the freestream velocity, whereas at AWC2 a spanwise velocity of up to 8% of the freestream velocity is observed.
A common feature of the different means of generating a secondary spanwise wave propagation is the formation of a ribbon-like pattern of streamwise vorticity near the wall, where the spanwise wavelength of the pattern corresponds with the spanwise wavelength of the excitation [2–5]. Figure 5 show the instantaneous distribution of the streamwise vorticity in a plane at $y^+ \approx 4$ above the actuated surface of AWC1 and AWC2, in which the ribbon-like formation of streamwise vorticity above the actuated walls can be seen. On the right-hand side of the figures the position of the surface is sketched to illustrate the corresponding wavelength of the surface wave. It is evident that the vorticity pattern and the surface motion do correlate. Therefore, at AWC1, where the friction drag is reduced by 9%, the spanwise structure possesses a larger well-ordered wavelength than the unactuated configuration and at AWC2 having a 8% higher friction drag the pattern is defined by a much smaller wavelength.

In Figure 6 the root-mean-square distributions of the streamwise ω'_x and wall-normal ω'_y vorticity fluctuations at $x/\delta_i = 155$ are given as a function of the wall-normal coordinate y^+ for the unactuated and actuated wall cases.
As discussed in [5] the overall increased streamwise vorticity fluctuations and the damped wall-normal vorticity fluctuations (Figure 6) are one of the main differences between the unactuated case and the AWC1 configuration. Considering the wall normal vorticity component distribution above the trough its variation with the wall motion corresponds to that of the wall-shear stress.
Du *et al.* [2] and Zhao *et al.* [3] also observed the damping of the wall-normal vorticity fluctuations. This damping and the reduction of friction drag supports the idea of a turbulence regeneration cycle for wall-bounded flows containing the streamwise and the wall-normal vorticity as proposed by Jiménez and Pinelli [13]. These authors performed a direct-numerical simulation (DNS) of a turbulent channel flow at moderate Reynolds numbers and found an increased streamwise vorticity and a decreased friction drag, when a filter function that damps the coherent components of the wall-normal vorticity in the near-wall regions was introduced. Also Schoppa and Hussain [14] determined the wall-normal vorticity to be a key indicator of streak instability and formation of new streaks.
It can be concluded that the introduction of a streamwise vorticity pattern is not sufficient to damp the turbulence regeneration cycle and as such to reduce the wall friction. It is the reduction of the wall-normal vorticity at every point in the near-wall flow field which correlates with a reduced turbulence regeneration cycle and hence with a reduced friction drag.
In a turbulent flat-plate boundary-layer flow over the unactuated wall the $\overline{u'v'}$ Reynolds stress component is known to dominate the production term P_k of the conservation equation of the turbulent kinetic energy $k = \frac{1}{2}\overline{u_i u_i}$. The production term

P_k for incompressible flows reads [15]

$$P_k = -\overline{u_i'u_j'}\frac{\partial \overline{u}_i}{\partial x_j} \quad . \tag{2}$$

The phase averaged turbulent production above the unactuated and actuated walls at a streamwise location of $x/\delta_i = 187$ is given in Figure 7. To non-dimensionalize the data the kinetic viscosity ν and the friction velocity u_τ of the unactuated wall case are used.

In the crest region the maximum occurring production is almost twice the production in the trough region. Note that the spanwise location which possesses the maximum turbulent kinetic energy production does not coincide with the location of the point of the maximum wall amplitude ($z^+ = 870$). At AWC2 the maximum turbulent kinetic energy production is about four times higher than that of the unactuated wall.

The production term of the k-equation is the sum of the production terms of the averaged fluctuation products $\overline{u'u'}$, $\overline{v'v'}$, and $\overline{w'w'}$. In Figure 8 the distribution of the production terms P_{uu}, P_{vv}, and P_{ww} is presented for both actuated wall cases. The distribution of the production P_{uu} at AWC2 is qualitatively like that at AWC1. The contribution of the production term P_{vv} is comparatively small. The distribution of the production term P_{ww} at AWC2 differs remarkably from that at AWC1. At AWC2 no negative production occurs and the maximum positive production exceeds the production at AWC1 by a factor of about 11. The production of the conservation equation of the turbulent kinetic energy P_k at AWC2 is dominated by P_{uu} and P_{ww} which leads to the distribution shown in Figure 7. Overall, it can be concluded that the wall actuation at AWC1 damps the production of the k-equation compared to the unactuated wall case, since the production is unchanged in the crest region and decreased in the trough region. At AWC2 the production of the k-equation is increased through the enhanced production of the P_{ww}-term. To determine the global effect of the wall actuation on the production term P_k, a spanwise averaging in the relative frame of references, where $y = 0$ is located at the position of the surface, is performed. The results, shown in Figure 9, evidence the damping of the turbulence production by the AWC1 setup and the amplified turbulence production by the AWC2 setup compared to the unactuated case.

Conclusion

Numerical simulations of a spatially evolving turbulent boundary layer impacted by spanwise traveling transversal surface waves were performed. Compared to an unactuated reference configuration a reduction of friction drag of about 9% was determined for a surface wave at a wavelength $\lambda^+ = 870$, a period $T^+ = 50$, and an amplitude $\hat{y}^+ = 30$, whereas a drag increase of about 8% was found at $\lambda^+ = 174$, $T^+ = 10$, and $\hat{y}^+ = 10$. The comparison of the two wave setups in the current study evidenced the key features to reduce friction drag at a wave-like excitation of the near-wall turbulence, i.e., a damping of wall-normal vorticity fluctuations over the surface. The formation of a ribbon-like pattern of streamwise vorticity were shown to not necessarily lower friction drag since they were observed not only in the drag decreasing wave setup but also in the drag increasing wave configuration.

Although the investigations concerning the application of an actuated wall to generate a spanwise transversal wave were originally initiated to only reduce friction drag, the current work reveals the possibility to depending on the wave pattern to also increase the turbulent production. An increased turbulent production is, for instance, beneficial to prevent boundary layer separation in an adverse-pressure gradient flow.

REFERENCES

[1] ACARE - Advisory Councilfor Aeronautic Research in Europe, *European Aeronautics: A Vision for 2020*. European Commission, 2001.

[2] Y. Du, V. Symeonidis, and G. E. Karniadakis, "Drag reduction in wall-bounded turbulence via a transverse travelling wave," *J. Fluid Mech.*, vol. 457, pp. 1–34, Apr. 2002.

[3] H. Zhao, J.-Z. Wu, and J.-S. Luo, "Turbulent drag reduction by traveling wave of flexible wall," *Fluid Dyn. Res.*, vol. 34, pp. 175–198, Mar. 2004.

[4] M. Itoh, S. Tamano, K. Yokota, and S. Taniguchi, "Drag reduction in a turbulent boundary layer on a flexible sheet undergoing a spanwise traveling wave motion," *J. Turbulence*, vol. 7, pp. 1–17, 2006.

[5] S. Klumpp, M. Meinke, and W.Schröder, "Drag reduction by spanwise transversal surface waves," *J. Turbulence*, vol. 11, no. 11, pp. 1–13, 2010.

[6] S. Klumpp, M. Meinke, and W.Schröder, "Friction drag variation by spanwise transversal surface waves," *Flow, Turbulence and Combustion*, no. DOI 10.1007/s10494-011-9326-3, 2011.

[7] J. P. Boris, F. F. Grinstein, E. S. Oran, and R. L. Kolbe, "New insights into large eddy simulation," *Fluid Dynamics Research*, vol. 10, pp. 199–228, 1992.

[8] M. S. Liou and C. J. Steffen Jr., "A new flux splitting scheme," vol. 107, pp. 23–39, 1993.

[9] M. Meinke, W. Schröder, E. Krause, and T. Rister, "A comparison of second- and sixth-order methods for large-eddy simulations," *Computers and Fluids*, vol. 31, pp. 695–718, 2002.

[10] N. Alkishriwi, M. Meinke, and W. Schröder, "A large-eddy simulation method for low mach number flows using preconditioning and multigrid," *Comp. Fluids*, vol. 35, no. 10, pp. 1126–1136, 2006.

[11] P. Renze, W. Schröder, and M. Meinke, "LES of turbulent mixing in film cooling flows," *Flow, Turbulence and Combustion*, vol. 80, pp. 119–132, 2008.

[12] W. El-Askary, W. Schröder, and M. Meinke, "LES of compressible wall-bounded flows," *AIAA Paper*, no. 2003-3554, 2003.

[13] J. Jiménez and A. Pinelli, "The autonomous cycle of near-wall turbulence," *J. Fluid Mech.*, vol. 389, pp. 335–359, June 1999.

[14] W. Schoppa and F. Hussain, "A large-scale control strategy for drag reduction in turbulent boundary layers," *Phys. Fluids*, vol. 10, pp. 1049–1051, May 1998.

[15] S. B. Pope, *Turbulent Flows*. Cambridge University Press, 2000.

Table 1. Grid parameters; L_x, L_y, and L_z denote the extensions and N_x, N_y, and N_z the grid points in the streamwise, the wall-normal, and the spanwise direction; the corresponding step sizes in each direction are given in wall units based on the flow state at point *m*.

Domain	$L_x/\delta_i \times L_y/\delta_i \times L_z/\delta_i$	$N_x \times N_y \times N_z$	Δx^+	Δy^+_{wall}	Δz^+
RS	$108 \times 35 \times 19.1$	$386 \times 71 \times 281$	14.2	0.9	3.1
AW unactuated	$231 \times 35 \times 19.1$	$761 \times 71 \times 281$	14.2	0.9	3.1
AW actuated	$231 \times 35 \times 19.1$	$793 \times 71 \times 281$	14.2	0.9	3.1

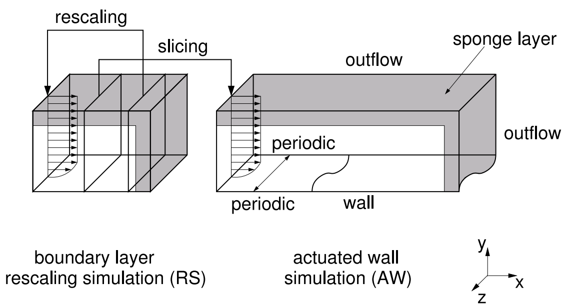

Figure 1. Computational domain.

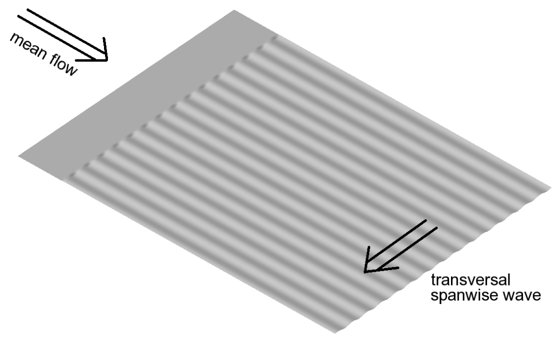

Figure 2. Flat-plate boundary-layer flow over a surface excited by transversal waves.

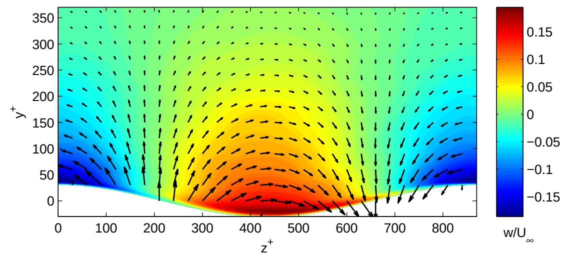

Figure 3. Phase averaged secondary flow above the actuated wall AWC1. Vectors consist of wall-normal and spanwise velocity components v and w with color coded spanwise velocity distribution.

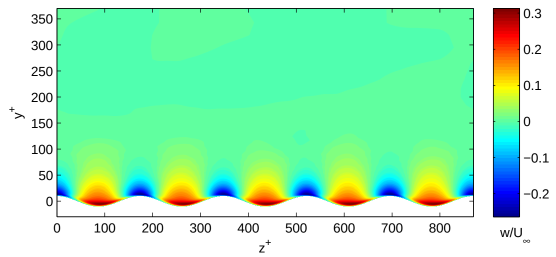

Figure 4. Phase averaged secondary flow above the actuated wall AWC2. Unlike at AWC1 (Figure 3) no vectors are shown for clarity with color coded spanwise velocity distribution.

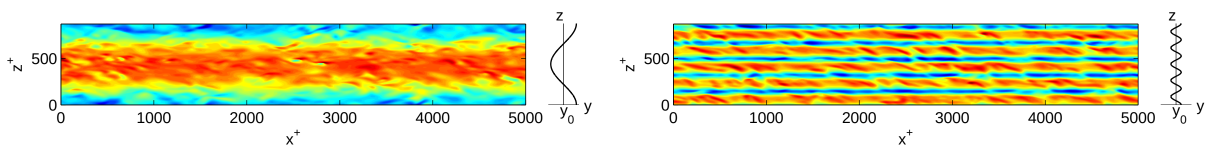

(a) (b)

Figure 5. Instantaneous streamwise vorticity fluctuations at $y^+ \approx 4$ above the actuated wall at AWC1 (a), and the actuated wall at AWC2 (b). The sketches on the right-hand side illustrate the wave pattern of the wall oscillation and the position y_0 of the non-moving wall.

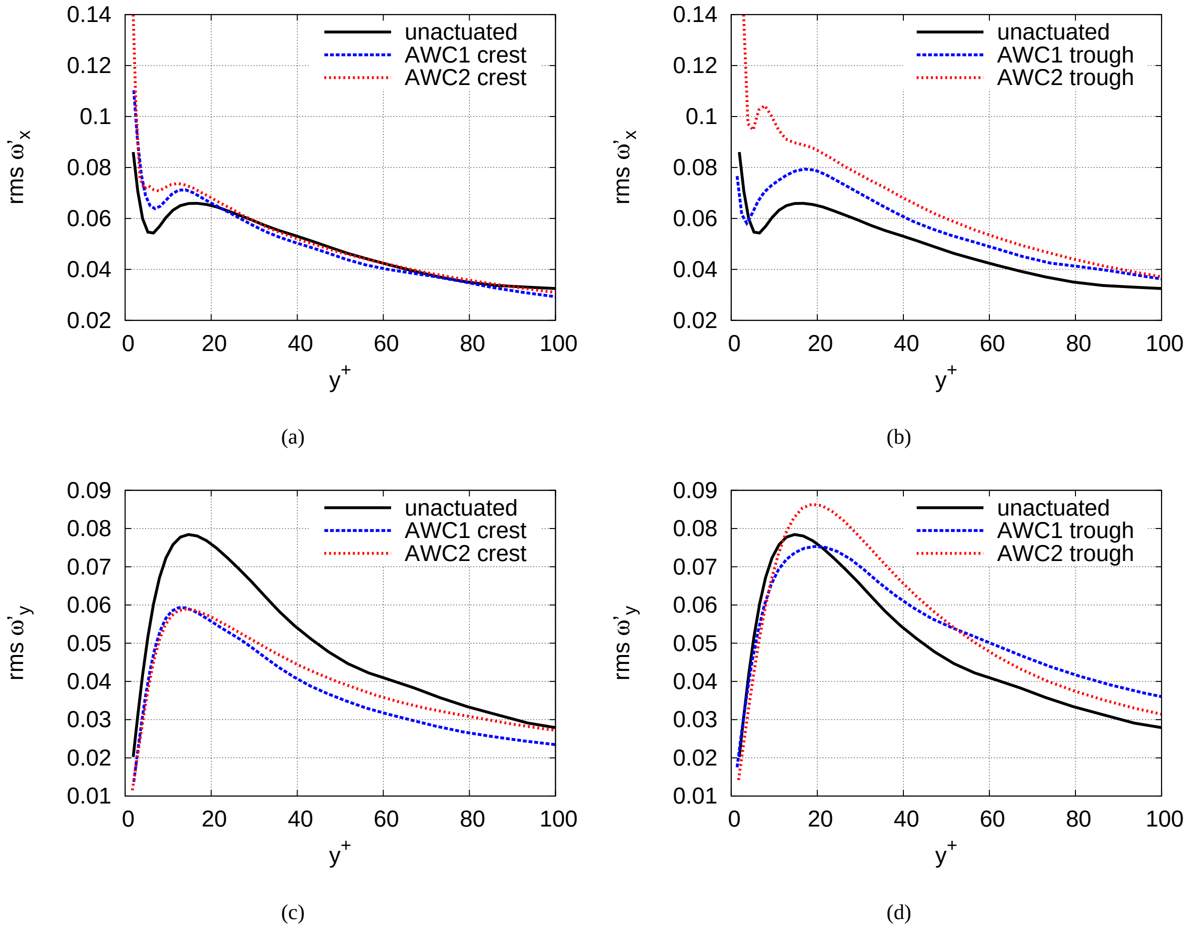

Figure 6. Root-mean-square (rms) distributions of the vorticity fluctuations in the streamwise and wall-normal direction for the unactuated case, AWC1, and AWC2 at the crest (left) and the trough (right).

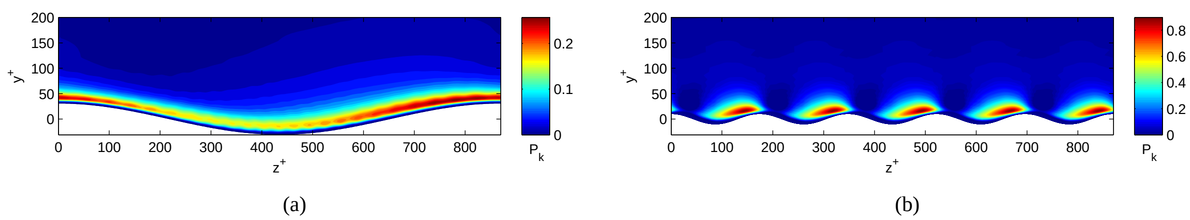

Figure 7. Phase averaged production term of the *k*-equation in a spanwise cross section above the actuated wall at AWC1 (a) and the actuated wall at AWC2 (b).

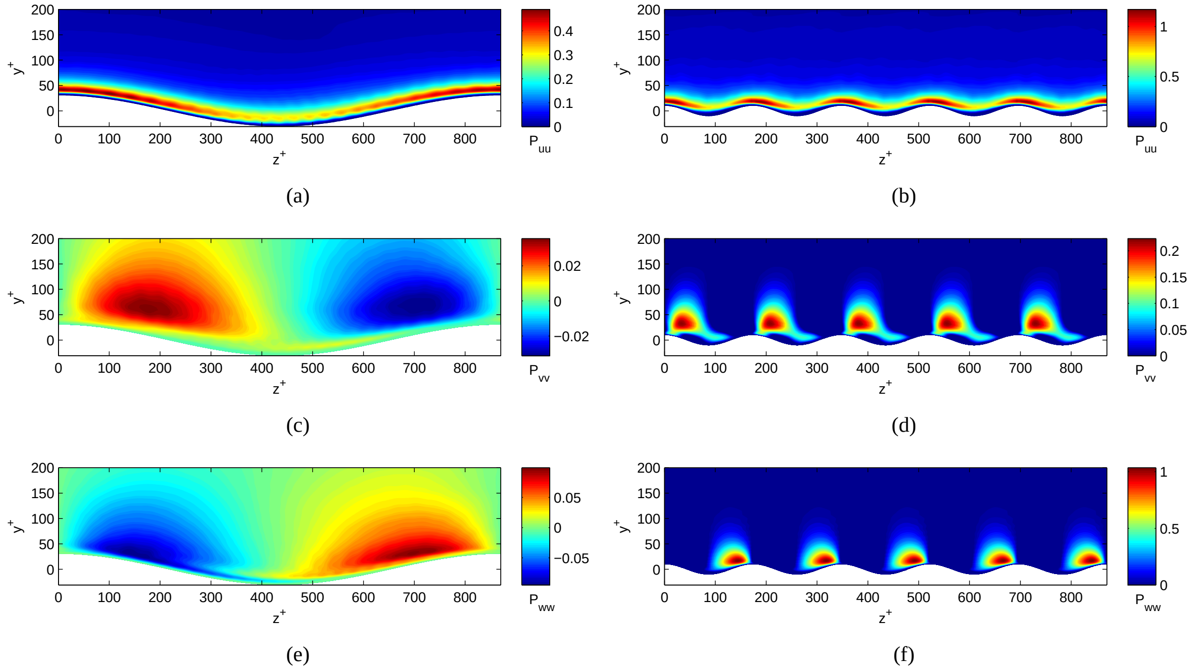

Figure 8. Phase averaged production term P_{uu}, P_{vv} and P_{ww} in a spanwise cross section above the actuated wall at AWC1 (a,c,e) and AWC2 (b,d,f).

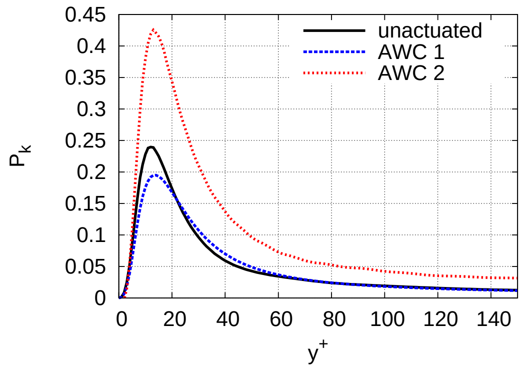

Figure 9. Spanwise averaged production term P_k.